

Low-energy enhancement of magnetic dipole radiation

R. Schwengner,¹ S. Frauendorf,² and A. C. Larsen³

¹*Institute of Radiation Physics, Helmholtz-Zentrum Dresden-Rossendorf, 01328 Dresden, Germany*

²*Department of Physics, University of Notre Dame, Notre Dame, Indiana 46556, USA*

³*Department of Physics, University of Oslo, 0316 Oslo, Norway*

(Dated: September 16, 2018)

Magnetic dipole strength functions have been deduced from averages of a large number of $M1$ transition strengths calculated within the shell model for the nuclides ^{90}Zr , ^{94}Mo , ^{95}Mo , and ^{96}Mo . An enhancement of $M1$ strength toward low transition energy has been found for all nuclides considered. Large $M1$ strengths appear for transitions between close-lying states with configurations including proton as well as neutron high- j orbits that re-couple their spins and add up their magnetic moments coherently. The $M1$ strength function deduced from the calculated $M1$ transition strengths is compatible with the low-energy enhancement found in $(^3\text{He}, ^3\text{He}')$ and (d, p) experiments. The present work presents for the first time an explanation of the experimental findings.

PACS numbers: 25.20.Dc, 21.10.Tg, 21.60.Jz, 23.20.-g, 27.50.+e

Photonuclear reactions and the inverse radiative-capture reactions between nuclear states in the region of high excitation energy and large level density, the so-called quasicontinuum of states, are of considerable interest in many applications. Radiative neutron capture, for example, plays a central role in the synthesis of the elements in various stellar environments [1, 2]. An improved theoretical description of neutron capture reactions is important for next-generation nuclear technologies, such as the transmutation of long-lived nuclear waste [1, 3]. Rates of these reactions are calculated using codes that are based on the statistical reaction theory (e.g. TALYS [4]). A critical input to these calculations is the average electromagnetic transition strengths, described by photon strength functions. For example, modifications of the electric-dipole ($E1$) strength function can cause drastic changes in the abundances of elements produced via neutron capture in the r -process occurring in violent stellar events [5].

In the energy range below about 10 MeV, which is relevant for the applications, the dipole strength function f_1 is dominated by the tail of the isovector electric giant dipole resonance (GDR), which is the collective vibration of the neutron system against the proton system. The damped vibration is described by a Lorentz shape to $f_1(E_\gamma)$ [6–8], where E_γ is the energy of the photon. Combinations of two or three Lorentz curves are used to describe the double or triple humps of the GDR caused by quadrupole and triaxial deformation of the nuclei [9–11]. Such a parametrization gives a good description of the experimental photoabsorption cross section $\sigma_\gamma = 3(\pi\hbar c)^2 E_\gamma f_1(E_\gamma)$ of nuclei in the ground state. It is quite common to adopt the so-called Brink-Axel hypothesis [6, 7], which states that the strength function does not depend on the excitation energy. This means that the same strength function describes the emission of photons from highly excited states, following e.g. neutron capture. The Generalized Lorentzian (GLO) [12] includes a

correction to the Standard Lorentzian (SLO) [6, 7], which accounts for the temperature of the nucleus emitting the photons.

For the magnetic dipole ($M1$) contribution to f_1 , two types of excitations have been considered so far. The scissors mode, which is interpreted as a small-amplitude rotation of the neutron system against the proton system, generates a bump of the $M1$ strength around 3 MeV in deformed nuclei [13]. After it had been well established in the absorption spectra of the ground state, it was recently also identified in the emission from highly excited states (see Ref. [14] and earlier work cited therein). At higher energy, typically around 8 MeV, the $M1$ strength is dominated by the spin-flip resonance [13]. Phenomenological $M1$ strength functions used in statistical-reaction codes are approximated by Lorentz curves with parameters usually derived from systematics [8].

The Lorentz curves used for the $E1$ and $M1$ strength functions decrease when approaching $E_\gamma = 0$. In contrast, an increase of the dipole strength function below 3 MeV toward low γ -ray energy has been found in several nuclides in the mass range from $A \approx 50$ to 100, such as $^{56,57}\text{Fe}$ [15], ^{60}Ni [16], and $^{105,106}\text{Cd}$ [17]. In particular, this low-energy enhancement of the strength function was deduced from experiments using $(^3\text{He}, ^3\text{He}')$ reactions on various Mo isotopes [18] and was confirmed in an independent experiment using the $^{94}\text{Mo}(d, p)^{95}\text{Mo}$ reaction [19]. The $(^3\text{He}, ^3\text{He}')$ data for ^{94}Mo , ^{95}Mo , and ^{96}Mo are shown in Figs. 1, 2, and 3, respectively, together with (γ, n) data [20]. The increase at low γ -ray energies may have a potentially large impact on neutron-capture reaction rates relevant for astrophysical processes [21]. Neither of these measurements were able to distinguish between $E1$ and $M1$ strength. An indication for an $M1$ character of the low-energy enhancement was discussed for the case of ^{60}Ni [16]. The γ -ray absorption from the ground state of even-even nuclei leads to only few discrete 1^+ and 1^- levels below 2 MeV. Obviously, it does

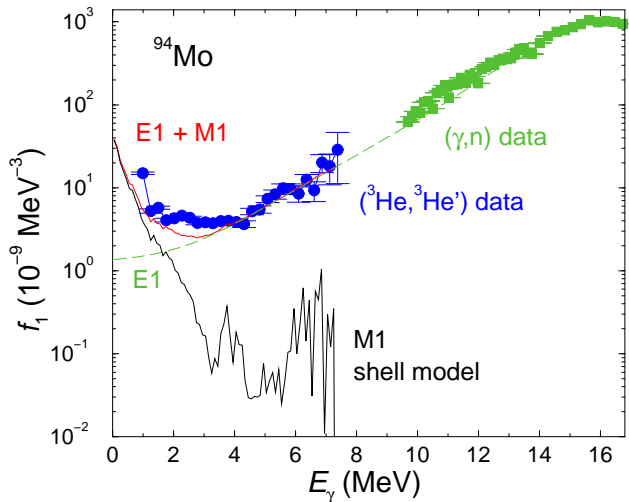


FIG. 1: (Color online) Strength functions for ^{94}Mo deduced from $(^3\text{He}, ^3\text{He}')$ (blue circles) and (γ, n) (green squares) experiments, the $M1$ strength function from the present shell model calculations (black solid line), $E1$ strength according to the GLO expression with parameters $E_0 = 16.36$ MeV, $\sigma_0 = 185$ b, $\Gamma = 5.5$ MeV, $T = 0.35$ MeV (green dashed line), and the total ($E1 + M1$) dipole strength function (red line).

not make sense to invoke the Brink-Axel hypothesis to relate these absorption cross sections to the observed low-energy enhancement of the γ -ray emission from highly excited levels. The properties of the $E1$ and $M1$ strength functions and their possible contributions to the strength function at very low energy are a challenging problem.

In this Letter we present shell-model calculations of the $M1$ strength function. We study the isotopes ^{94}Mo , ^{95}Mo , ^{96}Mo , in which the low-energy enhancement has been observed, and the $N = 50$ nuclide ^{90}Zr . A strong enhancement of the $M1$ transition strength is found below 2 MeV, which accounts for the observed enhancement. The mechanism that generates the strong low-energy $M1$ radiation will be explained.

The shell-model calculations were performed by means of the code RITSSCHIL [22] using a model space composed of the $\pi(0f_{5/2}, 1p_{3/2}, 1p_{1/2}, 0g_{9/2})$ proton orbits and the $\nu(0g_{9/2}, 1d_{5/2}, 0g_{7/2})$ neutron orbits relative to a ^{68}Ni core. The configuration space was tested in detail in our earlier shell-model studies of nuclei with $N = 46 - 54$ [23–37] and was found appropriate for the description of level energies as well as $M1$ and $E2$ transition strengths in nuclides around $A = 90$. As a further test, we compared the energies of yrast and yrare levels in $^{94,95,96}\text{Mo}$ and ^{90}Zr from the present calculation with the experimental ones, which agree within 300 keV.

The calculations included states with spins from $J =$

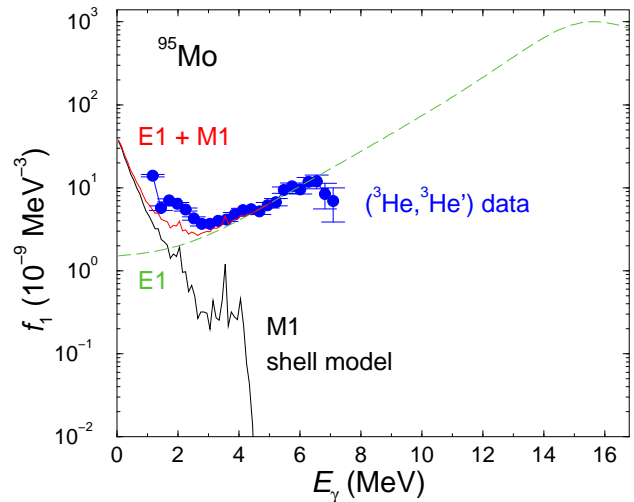


FIG. 2: (Color online) As Fig. 1, but for ^{95}Mo . (γ, n) data are not available for ^{95}Mo .

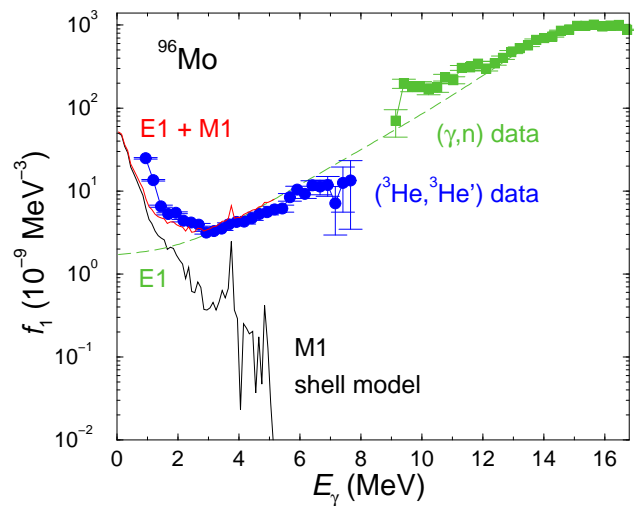


FIG. 3: (Color online) As Fig. 1, but for ^{96}Mo .

0 to 6 for ^{90}Zr , ^{94}Mo , ^{96}Mo , and from $J = 1/2$ to $13/2$ for ^{95}Mo . For each spin the lowest 40 states were calculated. The reduced transition probabilities $B(M1)$ were calculated for all transitions from initial to final states with energies $E_f < E_i$ and spins $J_f = J_i, J_i \pm 1$. For the minimum and maximum J_i , the cases $J_f = J_i - 1$ and $J_f = J_i + 1$, respectively, were excluded. This resulted in more than 14000 $M1$ transitions for each parity $\pi = +$ and $\pi = -$, which were sorted into 100 keV bins according to their transition energy $E_\gamma = E_i - E_f$. The

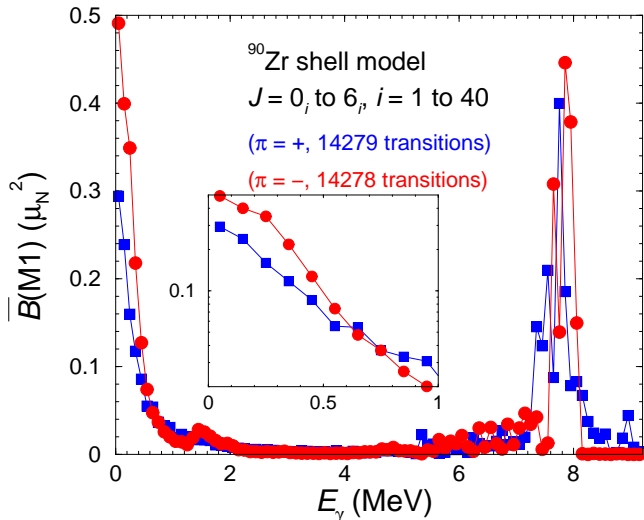


FIG. 4: (Color online) Average $B(M1)$ values in 100 keV bins of transition energy calculated for positive-parity (blue squares) and negative-parity (red circles) states in ^{90}Zr . The inset shows the low-energy part in logarithmic scale.

average $B(M1)$ value for one energy bin was obtained as the sum of all $B(M1)$ values divided by the number of transitions within this bin. The results for the nuclides ^{90}Zr and ^{94}Mo are shown in Figs. 4 and 5, respectively.

For all considered nuclides and each parity a pronounced low-energy enhancement of the average $\overline{B}(M1)$ values is seen. The bump around 7 MeV in ^{90}Zr and ^{94}Mo is caused by $1 \rightarrow 0$ and $0 \rightarrow 1$ transitions from states dominated by the spin-flip configuration $\nu(0g_{9/2}^{-1}0g_{7/2}^1)$. The cumulative strength calculated for the $1^+ \rightarrow 0_1^+$ transitions in ^{90}Zr is consistent with the value deduced in a recent experiment as shown in Ref. [38]. In ^{95}Mo and ^{96}Mo the bump around 7 MeV does not appear, because the excitation of a $1d_{5/2}$ neutron to the $0g_{7/2}$ orbit is preferred to $\nu(0g_{9/2}^{-1}0g_{7/2}^1)$.

The insets of Figs. 4 and 5 demonstrate that, up to 2 MeV, the low-energy enhancement of $\overline{B}(M1, E_\gamma)$ is well approximated by the exponential function $\overline{B}(M1, E_\gamma) = B_0 \exp(-E_\gamma/T_B)$ with $B_0 = \overline{B}(M1, 0)$ and T_B being constants. For the respective parities ($\pi = +, -$) we find for ^{90}Zr : $B_0 = (0.36, 0.58) \mu_N^2$ and $T_B = (0.33, 0.29)$ MeV, for ^{94}Mo : $B_0 = (0.32, 0.16) \mu_N^2$ and $T_B = (0.35, 0.51)$ MeV, for ^{95}Mo : $B_0 = (0.23, 0.12) \mu_N^2$ and $T_B = (0.39, 0.58)$ MeV, and for ^{96}Mo : $B_0 = (0.20, 0.13) \mu_N^2$ and $T_B = (0.41, 0.50)$ MeV.

To find out which states generate strong $M1$ transitions, the average $\overline{B}(M1)$ values for ^{94}Mo are plotted as a function of the energy of the initial states in Fig. 6. The large spike at 1.5 MeV in the distribution of $\pi = +$ states arises from the $2_2^+ \rightarrow 2_1^+$ and $4_2^+ \rightarrow 4_1^+$ transitions which link the main configurations $\nu(1d_{5/2}^2)$ in the 2_1^+ and

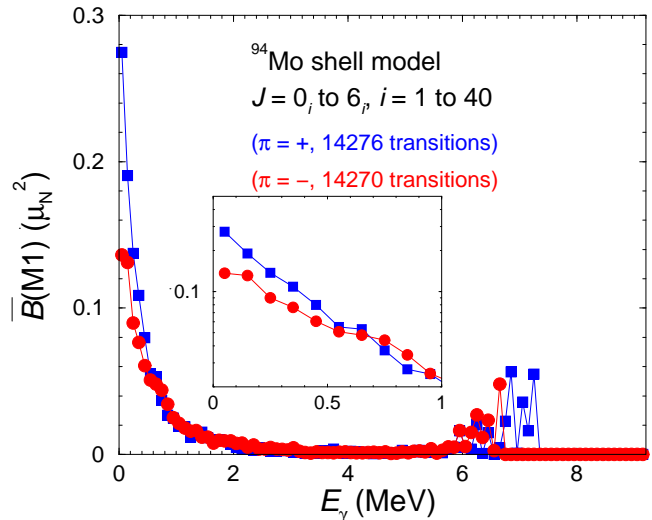


FIG. 5: (Color online) As Fig. 4, but for ^{94}Mo .

4_1^+ states with $\pi(0g_{9/2}^2)\nu(1d_{5/2}^2)$ in the 2_2^+ and 4_2^+ states. These findings are consistent with the experimental results given in Refs. [39, 40], which list $E_\gamma = 1196$ keV and $B(M1) = 0.56(5)\mu_N^2$ for the corresponding $2_3^+ \rightarrow 2_1^+$ transition to be compared with the calculated values of 884 keV and $0.96 \mu_N^2$. The bump in the $\pi = +$ distribution between 2 and 3 MeV includes among others the 1_2^+ state with the main configuration $\pi(0g_{9/2}^2)\nu(1d_{5/2}^2)$. It deexcites with $B(M1) = 0.37\mu_N^2$ to the ground state, comparable with the experimental 1_2^+ state described in Refs. [39, 40]. For ^{96}Mo there are analogous similarities of the calculations with the experimental results [41, 42]. The broad enhancements between 2 and 8 MeV (6 MeV) for the $\pi = +$ ($\pi = -$) distributions contain contributions from many states, where all included initial spins contribute approximately the same fraction. The $\overline{B}(M1)$ distributions versus E_i in ^{95}Mo and ^{96}Mo look similar to the ones in ^{94}Mo , but are shifted to somewhat lower excitation energy. In ^{90}Zr , the distributions start at about 3 MeV and continue to 10 MeV.

The low-energy enhancement of $M1$ strength is caused by transitions between many close-lying states of all considered spins located well above the yrast line in the transitional region to the quasi-continuum of nuclear states. Inspecting the wave functions, one finds large $B(M1)$ values for transitions between states that contain a large component (up to about 50%) of the same configuration with broken pairs of both protons and neutrons in high- j orbits. The largest $M1$ matrix elements connect configurations with the spins of high- j protons re-coupled with respect to those of high- j neutrons to the total spin $J_f = J_i, J_i \pm 1$. The main configurations are $\pi(0g_{9/2}^2)\nu(1d_{5/2}^2)$, $\pi(0g_{9/2}^2)\nu(1d_{5/2}^1 0g_{7/2}^1)$, and $\pi(0g_{9/2}^2)\nu(1d_{5/2}^2 0g_{9/2}^{-1} 0g_{7/2}^1)$ for positive-parity states in

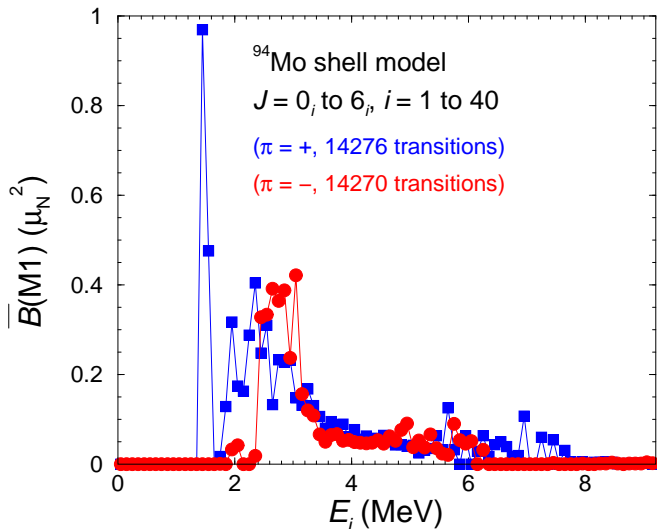


FIG. 6: (Color online) Average $B(M1)$ values in 100 keV bins of excitation energy calculated for positive-parity (blue squares) and negative-parity (red circles) states in ^{94}Mo .

^{94}Mo . Negative-parity states contain a proton lifted from the $1p_{1/2}$ to the $0g_{9/2}$ orbit in addition. In ^{90}Zr , analogous configurations are generated by exciting protons over the subshell gap at $Z = 40$ and neutrons over the shell gap at $N = 50$, i.e. $\pi(1p_{1/2}^{-2}0g_{9/2}^2)\nu(0g_{9/2}^{-1}1d_{5/2}^1)$ and $\pi(1p_{1/2}^{-2}0g_{9/2}^2)\nu(0g_{9/2}^{-1}0g_{7/2}^1)$ for positive-parity states and only one $1p_{1/2}$ proton lifted for negative-parity states. The orbits in these configurations have large g factors with opposite signs for protons and neutrons. Combined with specific relative phases of the proton and neutron partitions they cause large total magnetic moments.

The $M1$ strength functions were deduced using the relation $f_{M1}(E_\gamma) = 16\pi/9 (\hbar c)^{-3} \bar{B}(M1, E_\gamma) \rho(E_i)$. They were calculated by multiplying the $B(M1)$ value in μ_N^2 of each transition with 11.5473×10^{-9} times the level density at the energy of the initial state $\rho(E_i)$ in MeV^{-1} and deducing averages in energy bins as done for the $\bar{B}(M1)$ values (see above). The level densities $\rho(E_i, \pi)$ were determined by counting the calculated levels within energy intervals of 1 MeV for the two parities separately. For the Mo isotopes, the total level densities $\rho(E_i)$ are well reproduced by the constant-temperature expression $\rho(E_i) = \rho_0 \exp(E_i/T_\rho)$ as long as $E_i < 3$ MeV. For higher energies the combinatorial level density deviates from this expression and eventually decreases with excitation energy, which is obviously due to missing levels at high energy in the present configuration space. From a fit to the combinatorial values in the range $E_i < 2$ MeV we found for (ρ_0, T_ρ) in $(\text{MeV}^{-1}, \text{MeV})$ values of (1.37, 0.67), (1.90, 0.54), and (1.25, 0.58) for ^{94}Mo , ^{95}Mo , and ^{95}Mo , respectively. The level density in the semi-magic ^{90}Zr shows a more complicated energy dependence. The total $M1$ strength functions for ^{94}Mo , ^{95}Mo , and ^{96}Mo

are shown in Figs. 1, 2, and 3, respectively. As for the $B(M1)$, there is a pronounced enhancement below 2 MeV, which is well described by the exponential function $f_{M1}(E_\gamma) = f_0 \exp(-E_\gamma/T_f)$. For ^{90}Zr , ^{94}Mo , ^{95}Mo , and ^{96}Mo , the parameters are $f_0 = (34, 37, 39, 55) \times 10^{-9} \text{ MeV}^{-3}$ and $T_f = (0.50, 0.50, 0.51, 0.48) \text{ MeV}$, respectively.

To compare the calculated strength functions with the ones deduced from the $(^3\text{He}, ^3\text{He}')$ experiments of Ref. [18], the $E1$ contributions have to be added. Because a calculation of the $E1$ strength within the present model space is not possible, we adopted the GLO expression with parameters adjusted to (γ, n) data [20] and the $(^3\text{He}, ^3\text{He}')$ data above 4 MeV, where our $M1$ contribution is negligible. In the comparison, we focus on the low-energy region observed only via the $(^3\text{He}, ^3\text{He}')$ reaction, whereas there exist also other experimental data for energies above about 4 MeV [43]. As seen in Figs. 1, 2, and 3, the dipole strength functions found in the present calculations resemble the ones deduced from ^3He -induced reactions on $^{93-98}\text{Mo}$ [18, 21] and from a recent $^{94}\text{Mo}(d, p)^{95}\text{Mo}$ experiment [19], though the experimental data are available for $E_\gamma > 1$ MeV only. There is a certain freedom in determining the parameters for the GLO, which results in some uncertainty of the magnitude of the GLO in the enhancement region. As the GLO gives only a minor contribution to the total strength below $E_\gamma = 2$ MeV, an acceptable modification of the parameters will not remove the exponential enhancement caused by the $M1$ radiation. It will change the values around 2 MeV, leaving room for other possible enhancement mechanisms. The comparison suggests that at least part of the low-energy enhancement in the experimental dipole strength functions can be explained by $M1$ transitions in the quasi-continuum of states. The analogous low-energy enhancement predicted for ^{90}Zr suggests an experimental study of this nuclide.

Recent work [44] suggested that thermal coupling of quasiparticles to the continuum of unbound states may enhance the low-energy $E1$ strength. To account for the enhancement observed at 1 MeV, the temperature has to be above 1.4 MeV. This temperature is higher than temperatures predicted by the constant-temperature and Fermi-gas models (0.8 – 0.9 MeV) [49], the ones deduced from our shell-model level densities (0.6 MeV), and the experimental values (0.8 – 1.0 MeV) derived in Ref. [18]. In contrast to our $M1$ strength function, which peaks at zero energy, the $E1$ strength function has a maximum near 1 MeV and disappears at zero energy. The data in Figs. 1, 2, and 3 are compatible with a combination of both mechanisms, where the relative contribution to the low-energy enhancement cannot be assessed.

The re-coupling of spins leading to large $B(M1)$ values has been discussed in connection with high-spin multiplets (see, e.g. Refs. [23–26]). An analogous mechanism generates the “shears bands” manifesting “magnetic ro-

tation” [45], which was also observed in the mass-90 region [24, 46]. The “mixed-symmetry” configurations of the interacting boson model arise also from a reorientation of the proton angular momentum with respect to the neutron one. All these phenomena appear in nuclei near closed shells, if there are active high- j proton and neutron orbits near the Fermi surface with magnetic moments adding up coherently. Because these conditions are also prerequisites for the low-energy enhancement, one may expect it to appear in the same nuclei as the phenomena just mentioned. For example, the mixed-symmetry configurations discussed for ^{94}Mo [39, 40] and ^{96}Mo [41, 42] correspond to the dominating configurations $\pi(0g_{9/2}^2)\nu(1d_{5/2}^x)$ ($x = 2, 3, 4$ for $^{94,95,96}\text{Mo}$, respectively) that were found causing large $B(M1)$ strengths in the present calculations. The regions in the nuclear chart, where magnetic rotation is expected, are delineated in Fig. 22 of Ref. [45]. In fact, ^{90}Zr and the Mo isotopes discussed in the present work as well as the Fe, Ni, and Cd isotopes, for which the low-energy enhancement was observed [15–17], belong to these regions. On the other hand, ^{117}Sn [47], ^{158}Gd [48], and the Th, Pa isotopes [14], for which no low-energy enhancement was observed, lie outside these regions. In Ref. [21] it was demonstrated that a low energy-energy enhancement of the dipole strength function comparable with the present one for f_{M1} (GLOup2 in Ref. [21]) increases the astrophysical (n, γ) rate of the r-process by more than a factor of 10. A comparable increase may be expected for nuclei near the neutron drip line located in the mass regions around $(Z, N) = (22, 48), (26, 52), (34, 80), (64, 118)$, where magnetic rotation has been predicted and thus, the $M1$ strength should be enhanced at low energy.

Summarizing, the present shell-model calculations result in a large number of low-energy $M1$ transitions between excited states. Their average strength steeply increases toward zero transition energy. The strong radiation is generated by a reorientation of the spins of high- j proton and neutron orbits. This $M1$ radiation accounts for the enhancement of the dipole strength found in experiments. However, the uncertainties in calculating the low-energy $E1$ strength leave room for additional mechanisms.

We thank F. Dönau, H. Grawe, E. Grosse, and E. Litvinova for stimulating discussions. A. C. L. acknowledges support from the Research Council of Norway, project grant no. 205528, and S. F. acknowledges support by HZDR and by the DoE Grant DE-FG02-95ER4093.

- [2] F. Käppeler *et al.*, Rev. Mod. Phys. **83**, 157 (2011).
 [3] M. B. Chadwick. *et al.*, Nucl. Data Sheets **112**, 2887 (2011).
 [4] A. J. Koning, S. Hilaire, and M. C. Duijvestijn, AIP Conf. Proc. **769**, 1154 (2005).
 [5] S. Goriely, Phys. Lett. B **436**, 10 (1998).
 [6] D. M. Brink, Ph. D. thesis, Oxford University, 1955, unpublished.
 [7] P. Axel, Phys. Rev. **126**, 671 (1962).
 [8] R. Capote *et al.*, Nucl. Data Sheets **110**, 3107 (2009).
 [9] A. Bohr and B. R. Mottelson, *Nuclear structure, vol. II*, (W. A. Benjamin, Inc., Reading, Massachusetts, 1975).
 [10] J. M. Eisenberg and W. Greiner, *Nuclear theory, vol. I*, (North-Holland, Amsterdam, 1975).
 [11] A. R. Junghans *et al.*, Phys. Lett. B **670**, 200 (2008).
 [12] J. Kopecky and M. Uhl, Phys. Rev. C **41**, 1941 (1990).
 [13] K. Heyde, P. von Neumann-Cosel, and A. Richter, Rev. Mod. Phys. **82**, 2365 (2010).
 [14] M. Guttormsen *et al.*, Phys. Rev. Lett. **109**, 162503 (2012).
 [15] A. Voinov *et al.*, Phys. Rev. Lett. **93**, 142504 (2004).
 [16] A. Voinov *et al.*, Phys. Rev. C **81**, 024319 (2010).
 [17] A. C. Larsen *et al.*, Phys. Rev. C **87**, 014319 (2013).
 [18] M. Guttormsen *et al.*, Phys. Rev. C **71**, 044307 (2005).
 [19] M. Wiedeking *et al.*, Phys. Rev. Lett. **108**, 162503 (2012).
 [20] H. Beil *et al.*, Nucl. Phys. **A227**, 427 (1974).
 [21] A. C. Larsen and S. Goriely, Phys. Rev. C **82**, 014318 (2010).
 [22] D. Zwarts, Comput. Phys. Commun. **38**, 365 (1985).
 [23] R. Schwengner *et al.*, Phys. Rev. C **80**, 044305 (2009).
 [24] R. Schwengner *et al.*, Phys. Rev. C **66**, 024310 (2002).
 [25] R. Schwengner *et al.*, Nucl. Phys. **A584**, 159 (1995).
 [26] R. Schwengner *et al.*, Phys. Rev. C **57**, 2892 (1998).
 [27] R. Schwengner *et al.*, Phys. Rev. C **74**, 034309 (2006).
 [28] G. Winter *et al.*, Phys. Rev. C **48**, 1010 (1993).
 [29] G. Winter *et al.*, Phys. Rev. C **49**, 2427 (1994).
 [30] J. Reif *et al.*, Nucl. Phys. **A587**, 449 (1995).
 [31] E. A. Stefanova *et al.*, Phys. Rev. C **62**, 054314 (2000).
 [32] Y. H. Zhang *et al.*, Phys. Rev. C **70**, 024301 (2004).
 [33] A. Jungclaus *et al.*, Nucl. Phys. **A637**, 346 (1998).
 [34] A. Jungclaus *et al.*, Phys. Rev. C **60**, 014309 (1999).
 [35] E. A. Stefanova *et al.*, Phys. Rev. C **63**, 064315 (2001).
 [36] G. Rainovski *et al.*, Phys. Rev. C **65**, 044327 (2002).
 [37] E. A. Stefanova *et al.*, Phys. Rev. C **65**, 034323 (2002).
 [38] G. Rusev *et al.*, Phys. Rev. Lett. **110**, 022503 (2013).
 [39] N. Pietralla *et al.*, Phys. Rev. Lett. **83**, 1303 (1999).
 [40] C. Fransen *et al.*, Phys. Rev. C **67**, 024307 (2003).
 [41] C. Fransen *et al.*, Phys. Rev. C **70**, 044317 (2004).
 [42] S. R. Leshner *et al.*, Phys. Rev. C **75**, 034318 (2007).
 [43] G. Rusev *et al.*, Phys. Rev. C **79**, 061302(R) (2009).
 [44] E. Litvinova and N. Belov, Phys. Rev. C **88**, 031302(R) (2013).
 [45] S. Frauendorf, Rev. Mod. Phys. **73**, 463 (2001).
 [46] H. Schnare *et al.*, Phys. Rev. Lett. **82**, 4408 (1999).
 [47] U. Agvaanluvsan *et al.*, Phys. Rev. Lett. **102**, 162504 (2009).
 [48] A. Chyzh *et al.*, Phys. Rev. C **84**, 014306 (2011).
 [49] T. von Egidy and D. Bucurescu, Phys. Rev. C **80**, 054310 (2009).